Electron-impact dissociative ionization of SF_6 studied by angle-resolved $(e, e + \text{ion})$ spectroscopy

Noboru Watanabe * and Masahiko Takahashi
Institute of Multidisciplinary Research for Advanced Materials, Tohoku University, Sendai 980-8577, Japan

(Received 24 June 2023; accepted 8 September 2023; published 19 October 2023)

We study the electron-impact dissociative ionization of SF_6 using a scattered electron-ion coincidence technique. The ion-yield spectra are obtained at an incident electron energy of 1.4 keV for scattering angles ranging from 2.2° to 8.2° to investigate the momentum transfer dependences of the fragment-ion yields and shape resonance features. It is found that the $4t_{1u} \rightarrow \varepsilon t_{2g}$ resonance is evident over a wide momentum transfer range, indicating its strong influence on the SF_3^+ production by electron impact, while resonance bands in the SF_5^+ and SF_4^+ yield spectra rapidly diminish with increasing momentum transfer. In addition, the angular distribution of SF_5^+ reveals the significant difference in stereodynamics between electron-impact-induced and photon-induced ionization of SF_6. We also discuss the dissociation mechanisms of SF_6^+ using the kinetic energy distributions of the fragment ions. Analysis of the data strongly suggests that many of the SF_6^+ ions in the $D\ ^2T_{2g}$ state decay by internal conversion to a lower electronic state and dissociate to $SF_5^+ + F$, followed by statistical emission of F or F_2.

DOI: 10.1103/PhysRevA.108.042814

I. INTRODUCTION

Sulfur hexafluoride (SF_6) is a fluorine-containing molecule, widely used for dry plasma etching in the semiconductor industry [1–4]. Understanding the physical and chemical processes involved in plasma etching with this molecule requires proper knowledge of the electron-impact ionization and subsequent molecular fragmentation of SF_6 [3,4]. This molecule is also used as an insulating medium in high-voltage electrical equipment. Because of this practical importance, the interaction of electrons with SF_6 has been the subject of a number of studies [4,5]. In addition, the electron- and photon-induced ionization of SF_6 has received much attention due to the appearance of prominent shape resonance features in the individual ionization channels [6–11]. The resonance, which is attributed to a barrier formed in the effective molecular potential, is not only of interest from the point of view of molecular spectroscopy, but also has a significant influence on the ionization cross sections and the product ion branching ratio.

Owing to its fundamental importance in molecular physics, the photodissociative ionization of SF_6 has been investigated using a variety of experimental techniques. The partial photoionization cross sections have been obtained using time-of-flight mass spectroscopy with dipole electron scattering or synchrotron radiation [12,13]. The kinetic energy release for SF_6 through the two lowest states of SF_6^+ was reported by an early photoelectron-photoion coincidence study [14], and the molecular fragmentation of SF_6^+ was studied using a photoionization mass spectroscopy technique [15]. Later, the branching ratio of the fragment ions and the mean kinetic energy release for each ionic state were measured by means of threshold photoelectron-photoion coincidence (TPEPICO) spectroscopy [16,17]. Additionally, a photofragment imaging technique was adopted to study the dissociative ionization dynamics of SF_6 [18].

A major difference between photon-induced and electron-induced processes is that while the former leads to the electric dipole transitions of molecules, the latter causes not only electric dipole but also electric quadrupole and higher-order multipole transitions [19]. Despite its importance for understanding the dynamics of electron-impact dissociative ionization of SF_6, knowledge of the nondipole ionization and subsequent molecular fragmentation is scarce. Angle-resolved electron energy loss spectroscopy (EELS) provides a powerful tool for studying nondipole transitions in molecules [19–21]. By measuring the momentum transfer dependence of the electron scattering cross sections, one can elucidate the nature of individual electronic excitations, and this technique has indeed been applied to the study of the valence [22,23] and inner-shell [7,24] excitations in SF_6. Nevertheless, while the EELS studies have provided detailed insight into the discrete excitations, this is not always the case for the dissociative ionization; the contributions of the individual ionization channels to the scattering cross section cannot be completely separated in the experiment, and furthermore, no information about the subsequent dissociation processes can be obtained from the EELS data alone. With respect to the dissociation processes, the relative ion yields and ion kinetic energy distributions carry information about the branching ratio of the decay channels and molecular fragmentation mechanisms. The partial-ionization cross sections and kinetic energy distributions of all major ion products were therefore measured for the electron-impact ionization of SF_6 by Bull *et al.* using a velocity map imaging technique [25]. However, since the scattered electrons were not detected in the experiments, the energy transferred from the incident electron to the molecule

*noboru.watanabe.e2@tohoku.ac.jp

could not be defined, making the results difficult to interpret. In this context, if the EELS technique could be combined with a fragment-ion momentum imaging measurement, more detailed information on electron-impact dissociative ionization could be obtained.

Recently, we have developed a scattered electron-ion coincidence technique and applied it to the study of the stereodynamics of electron-impact ionization of linear molecules [26–30]. In this so-called (e, e + ion) experiment, the energies and momenta of the scattered electrons and fragment ions are fully determined, allowing us to measure the angular and kinetic energy distributions of the ion products for given electron energy loss and momentum transfer. The (e, e + ion) technique thus provides a good opportunity to investigate the electron-impact dissociative ionization of SF_6 in much more detail than previously possible. In this work (e, e + ion) experiments have been carried out for the valence ionization of SF_6. The total and partial ion-yield spectra are constructed from the results measured at different momentum transfers to investigate the change in the fragment ion yields due to the influence of higher-order multipole interactions. An examination of the shape resonance bands in the spectra shows that the $4t_{1u} \rightarrow \varepsilon t_{2g}$ transition has a significant influence on the formation of SF_3^+ over a wide momentum transfer range. Furthermore, the electron energy loss dependence of the ion kinetic energy distributions has been examined to gain insight into the dissociation mechanisms of SF_6^+ produced by electron impact.

II. EXPERIMENT

Within the framework of the Born approximation, the differential electron scattering cross section is expressed as follows [19,20]:

$$\frac{d^2\sigma}{d\Omega dE} = \frac{|\boldsymbol{k}_s|}{|\boldsymbol{k}_i|}\frac{2}{|\boldsymbol{K}|^2 E}\frac{df(\boldsymbol{K},E)}{dE}. \tag{1}$$

Here $\boldsymbol{k}_i$ and $\boldsymbol{k}_s$ are the momenta of the incident and scattered electrons, $\boldsymbol{K}$ ($\boldsymbol{k}_i$–$\boldsymbol{k}_s$) is the momentum transfer, and E is the electron energy loss. Hartree atomic units are used here. The last term in Eq. (1) denotes the generalized oscillator strength (GOS) for a transition from the initial ground state:

$$\frac{df(\boldsymbol{K},E)}{dE} = \frac{2E}{K^2}\sum_n |\langle\Phi_n|\sum_j \exp(i\boldsymbol{K}\cdot\boldsymbol{r}_j)|\Phi_0\rangle|^2 \delta(E-E_{n0}), \tag{2}$$

where $\boldsymbol{r}_j$ is the position of the jth electron and E_{n0} is the energy difference between the initial target state Φ_0 and an excited state Φ_n. In the limit as K (= $|\boldsymbol{K}|$) approaches zero, the exponential term in Eq. (2) can be approximated as $\exp(i\boldsymbol{K}\cdot\boldsymbol{r}_j) = 1 + i\boldsymbol{K}\cdot\boldsymbol{r}_j$ and the GOS thus converges to the optical oscillator strength (OOS) [19,20], which can be obtained also by photoabsorption.

$$\lim_{K\to 0}\frac{df(\boldsymbol{K},E)}{dE} = 2E\sum_n |\langle\Phi_n|\sum_j \hat{\boldsymbol{K}}\cdot\boldsymbol{r}_j|\Phi_0\rangle|^2 \delta(E-E_{n0}). \tag{3}$$

Here $\hat{\boldsymbol{K}}$ is a unit vector along $\boldsymbol{K}$; it plays a role equivalent to the light polarization vector in photoabsorption. Note that while electric dipole transitions are dominant at $K \sim 0$, effects of higher-order multipole interactions become larger with the increase in K.

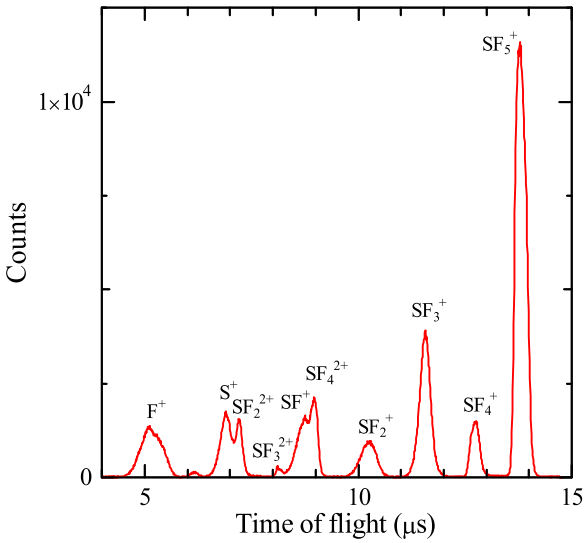

FIG. 1. Time-of-flight spectrum of SF_6.

To obtain partial GOSs for fragment-ion formation, we performed electron-ion coincidence measurements using an (e, e + ion) spectrometer. A detailed description of the spectrometer has been given elsewhere [31] and will not be repeated here. Briefly, it consists of an electron gun, an energy dispersive electron spectrometer, and an ion momentum imaging spectrometer. An electron beam from the electron gun is chopped at a frequency of 62.5 kHz by the application of voltage pulses to a deflection electrode, and then crossed with an effusive molecular beam. Electrons scattered at an angle of θ with respect to the electron beam direction are dispersed by a hemispherical analyzer and directed to a position-sensitive detector. The scattering angle is related to the magnitude of the momentum transfer as $K = (k_i^2 + k_s^2 - 2|\boldsymbol{k}_i||\boldsymbol{k}_s|\cos\theta)^{1/2}$. When an electron is detected, a pulsed electric field is applied to the scattering region to extract ions into the momentum imaging spectrometer. The ions are projected onto a position- and time-sensitive microchannel plate (MCP) detector equipped with delay-line anodes.

Experiments were performed at an impact energy of E_0 = 1.4 keV for $\theta = 2.2°$, 4.6°, 6.0°, and 8.2° (K^2 = 0.16, 0.67, 1.13, and 2.10 a.u.). High-purity SF_6 gas (> 99.999%) supplied by Japan Fine Products was used for the measurements. The energy resolution for electrons was estimated to be 0.8 eV, which is the full width at half maximum from the peak profile of the elastic scattering. The recoil momentum of each ion was derived from its time of flight (TOF) and arrival position at the MCP detector. The momentum resolution is mainly determined by the translational temperature of the target molecules. The kinetic energy distributions of fragment ions obtained from the measurements are thus slightly broadened by the thermal energy of the molecules at a temperature of T = 295 K, ∼ 0.038 eV. Figure 1 shows the TOF spectrum of SF_6 measured with the momentum imaging spectrometer. The SF_6^+ parent ion is not observed in the spectrum because it is unstable and dissociates. Since the TOF peaks of SF^+ and SF_4^{2+} overlap considerably and cannot be resolved, the sum

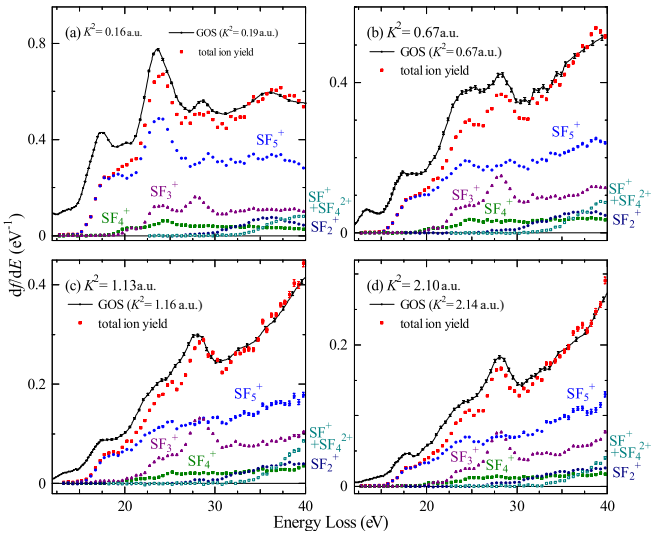

FIG. 2. Partial GOSs for formation of ions from SF_6 at K^2 = (a) 0.16, (b) 0.67, (c) 1.13, and (d) 2.10 a.u. Our previously reported GOS distributions [23] are included in the figure for comparison.

of their intensities is considered below. Electron-ion coincidence data were obtained by accumulating data at an ambient sample gas pressure of 1×10^{-4} Pa.

III. RESULTS AND DISCUSSION

A. Ion-yield spectra

Figure 2 shows the ion-yield spectra of SF_6. They were obtained by plotting the number of electron-ion coincidence signals against the electron energy loss E and converting to the partial GOS using the Bethe-Born formula [Eq. (1)]. Since the ionization efficiency of SF_6 is almost 1 above $E \sim 34$ eV [12], the partial GOS for total ion production should practically coincide with the GOS itself in the high-E region. Based on this, the total ion-yield spectra were placed on an absolute scale in the following manner. First, we obtained the integrated intensity of our previously reported GOS distribution [23] in the region from 34 to 40 eV and derived its momentum transfer dependence. Then each of the total ion-yield spectra was scaled so that the intensity of the 34–40 eV region was equal to that of the GOS distribution at the corresponding K^2. The resulting scaling factor was also applied to the partial ion-yield spectra to place them on the same absolute scale. The error bars in Fig. 2 show only the statistical uncertainties. From the reproducibility of the data, the overall uncertainties of the partial GOS values are estimated to be less than 13% and 8% for $\theta = 8.2^\circ$ and the other scattering angles, respectively. Figure 2 includes the GOS distributions at momentum transfers close to those of the present measurements. The total ion-yield spectra show good agreement in shape with the GOS distributions at large E, supporting the validity of the assumption that SF_6 is fully ionized above ~ 34 eV. The obtained partial GOS distributions tell us how the ion yields depend on the electron energy loss and momentum transfer.

The total ion-yield spectra show two broad bands with maxima at $E \sim 24$ and 28 eV, which may be due to shape resonance. These bands have been observed also in the EELS spectra of SF_6 and their plausible assignments have been proposed by Ying *et al.* [22]. However, it is not practically possible to make unambiguous assignments of the spectral features from the EELS data alone, because ionization from multiple valence orbitals ($1t_{1g}$, $5t_{1u}$, $1t_{2u}$, $3e_g$, $1t_{2g}$, $4t_{1u}$, and $5a_{1g}$) contributes to the electron scattering in the E region of interest. Moreover, the overlap of resonance features in the energy loss spectrum prevents one from assessing the momentum transfer dependence of each shape resonance band. Since the branching ratio into each fragment product depends on the state of SF_6^+ formed by electron impact, the electron-ion coincidence data can be used to partially separate the contributions from the individual ionization channels. Table I lists the ion products from each SF_6^+ state, measured by Creasey *et al.* [16] and Stankiewicz *et al.* [17] using the TPEPICO technique, together with the vertical ionization energies reported in the literature [32]. Since the $^2T_{1u}$ $(5t_{1u})^{-1}$ and $^2T_{2u}$ $(1t_{2u})^{-1}$ ionic states, or the A and B states, are so close in energy that their contributions cannot be separated [6], we denote them together as $\{A, B, {}^2T_{1u}, {}^2T_{2u}\}$.

TABLE I. Fragment ions produced from each ionization channel and the vertical ionization potentials. The # mark indicates that the branching ratio is small.

State	Orbital	Ionization potential (eV) [32]	Fragment ions [16,17]
$X\ ^2T_{1g}$	$1t_{1g}$	15.7	SF_5^+
$\{A, B, {}^2T_{1u}, {}^2T_{2u}\}$	$5t_{1u}$, $1t_{2u}$	17.0	SF_5^+
$C\ ^2E_g$	$3e_g$	18.6	SF_5^+, SF_4^+ [#,a]
$D\ ^2T_{2g}$	$1t_{2g}$	19.8	SF_5^+ [#], SF_4^+, SF_3^+ [b]
$E\ ^2T_{1u}$	$4t_{1u}$	22.6	SF_3^+
$F\ ^2A_{1g}$	$5a_{1g}$	26.8	SF_3^+ [c], SF_2^+

[a]The ratio of SF_4^+ and SF_5^+ is about 1:8 [16].
[b]The SF_5^+, SF_4^+, and SF_3^+ branching ratio is reported to be 1.0:2.0:1.8 [16].
[c]Reference [17].

The TPEPICO studies have shown that all of SF_6^+ ions in the $X\ ^2T_{1g}$ $(1t_{1g})^{-1}$, $\{A, B, {}^2T_{1u}, {}^2T_{2u}\}$ states and most of those in the $C\ ^2E_g$ $(3e_g)^{-1}$ state dissociate into $SF_5^+ + F$. Thus the partial GOS for SF_5^+ formation is mainly the contribution from the first four ionization channels, while it also contains a small contribution from the next channel, $D\ ^2T_{2g}$ $(1t_{2g})^{-1}$. The $D\ ^2T_{2g}$ ionization can be highlighted by selecting the electron-SF_4^+ coincidence signals, since SF_4^+ ions are formed predominantly from the $D\ ^2T_{2g}$ state, though some of them come from the $C\ ^2E_g$ state. The $D\ ^2T_{2g}$ state also decays to SF_3^+, and the $E\ ^2T_{1u}$ $(4t_{1u})^{-1}$ state yields exclusively SF_3^+, indicating that the SF_3^+ yield spectra can be associated with the $D\ ^2T_{2g}$ and $E\ ^2T_{1u}$ channels. Indeed, the SF_3^+ yield starts at ~ 19.3 eV, close to the vertical ionization energy of the $D\ ^2T_{2g}$ channel, and the intensity increases sharply near the $E\ ^2T_{1u}$ ionization energy. Besides, the later TPEPICO study by Stankiewicz *et al.* [17] has shown that SF_3^+ is formed also from the $F\ ^2A_{1g}$ $(5a_{1g})^{-1}$ state, and its contribution may be included in the SF_3^+ yield spectra above the ionization energy of 26.8 eV. The $F\ ^2A_{1g}$ state also decays to form SF_2^+, and thus the threshold for producing SF_2^+ is close

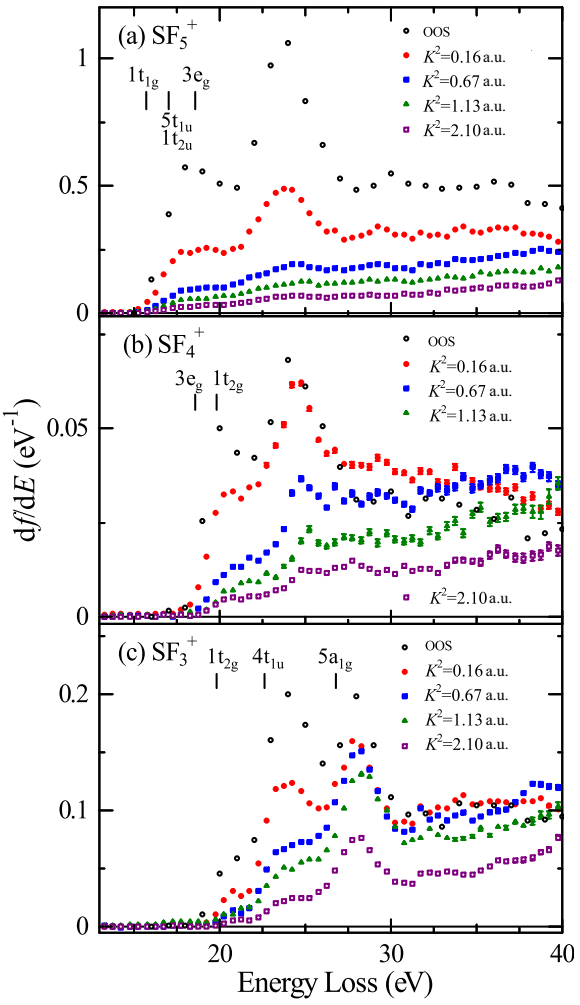

FIG. 3. Partial GOSs for formation of (a) SF_5^+, (b) SF_4^+, and (c) SF_3^+ ions from SF_6. Open circles are the partial OOSs reported by Hitchcock and van der Wiel [12], which correspond to the data at $K = 0$.

to the corresponding ionization energy. With the above discussion in mind, the partial ion-yield spectra are examined below.

The SF_5^+, SF_4^+, and SF_3^+ yield spectra, in which shape resonance features are observed, are plotted in Fig. 3, together with the partial OOSs reported by Hitchcock and van der Wiel [12], corresponding to the data at $K^2 = 0$. The vertical bars indicate the associated ionization energies. It can be seen from Fig. 3(a) that the partial GOS for SF_5^+ formation decreases rapidly with the increase of K^2, indicating a steady decrease of the sum of the $X\ ^2T_{1g}$, $\{A, B, ^2T_{1u}, ^2T_{2u}\}$, and $C\ ^2E_g$ ionization cross sections with momentum transfer. Also seen from the figure is that the spectra exhibit a broad band with a maximum at ~ 24 eV. A similar band has been observed in the photoionization cross section of the $5t_{1u}$ and $1t_{2u}$ subshells [6] and was attributed to the $5t_{1u} \rightarrow \varepsilon t_{2g}$ and $1t_{2u} \rightarrow \varepsilon t_{2g}$ shape resonance [6,8,9]. In addition, it has been reported that the $3e_g \rightarrow \varepsilon t_{1u}$ shape resonance appears around 22 eV in the $3e_g^{-1}$ ionization cross section [9]. Thereby, the broad band at ~ 24 eV can be ascribed to the $5t_{1u}$, $1t_{2u} \rightarrow \varepsilon t_{2g}$ and $3e_g \rightarrow \varepsilon t_{1u}$ transitions. This shape resonance band is found to be less pronounced with the increase of K^2. It is a typical behavior for dipole-allowed transitions [20].

It can be seen from Fig. 3(b) that the SF_4^+ yield spectra show a broad peak at ~ 25 eV. Since SF_4^+ ions are mainly generated from the $D\ ^2T_{2g}$ state, the broad peak can be attributed to the $1t_{2g} \rightarrow \varepsilon t_{1u}$ shape resonance, identified in the $D\ ^2T_{2g}$ photoionization cross section [9]. The theoretical study by Jose *et al.* [9] has revealed that interchannel coupling effects have a significant influence on the location and intensity of this shape resonance band. The intensity of the $1t_{2g} \rightarrow \varepsilon t_{1u}$ peak decreases with the increases of momentum transfer, as in the case of the 24 eV band in the SF_5^+ yield spectra.

We turn our attention to the SF_3^+ yield spectra in Fig. 3(c), associated with the $D\ ^2T_{2g}$, $E\ ^2T_{1u}$, and $F\ ^2A_{1g}$ channels. Owing to the contribution from the $D\ ^2T_{2g}$ channel, the SF_3^+ yield spectra should have a peak around 25 eV caused by the $1t_{2g} \rightarrow \varepsilon t_{1u}$ shape resonance. Indeed, a broad band is evident at $E \sim 24$ eV for $K^2 = 0.16$ a.u. A slight difference of the peak position may be due to the overlap of the $E\ ^2T_{1u}$ pre-edge structure in the lower-energy side. The band intensity quickly decreases with K^2, being consistent with the result for SF_4^+.

The SF_3^+ yield spectra also exhibit a broad band at ~ 28 eV. This band has been observed in angle-resolved EELS spectra and preliminarily assigned to the $4t_{1u} \rightarrow \varepsilon t_{2g}$ shape resonance [22]. This assignment is confirmed by the fact that the 28 eV band appears only in the SF_3^+ yield spectra, since the $E\ ^2T_{1u}\ (4t_{1u})^{-1}$ state yields exclusively SF_3^+. Of interest is that the band is quite evident even at large K^2, unlike the other shape resonance bands, which rapidly diminish with increasing K^2. The result indicates a crucial role of electric quadrupole and/or higher-order multipole interactions in the $4t_{1u} \rightarrow \varepsilon t_{2g}$ shape resonance. It has a considerable impact on the branching ratio into the SF_5^+ and SF_3^+ products at nonzero momentum transfer. As can be seen from Fig. 2, the emission intensity of SF_3^+ around the $4t_{1u} \rightarrow \varepsilon t_{2g}$ peak is comparable to that of SF_5^+ for $K^2 \geqslant 0.67$ a.u., while SF_5^+ is the predominant product in other scattering conditions investigated.

B. Kinetic energy distributions of ions

To gain insight into the dissociation mechanisms of SF_6^+, the kinetic energy (KE) distributions of the fragment ions are examined. The electron$-SF_n^+$ coincidence signals for $n = 5$, 4, and 3 are plotted against E and KE in Figs. 4–6, respectively. For a quantitative assessment of the E dependence, the KE distributions in several E regions are also shown in the lower panel of each figure. They are normalized by the maximum intensities for ease of comparison. While some K^2 dependence was observed for the E-KE correlation maps, it can be attributed simply to the change in relative contributions from different ionization channels with K^2, and thus only the data at $K^2 = 0.16$ a.u. are presented here.

It can be seen from Fig. 4 that the KE distribution of SF_5^+ does not vary significantly with E. In particular, the distributions at $E > 18$ eV are nearly coincident with a maximum at ~ 0.16 eV and extending to about 0.6 eV. While shape resonance is observed in the SF_5^+ yield spectrum at ~ 24 eV, it has no noticeable effect on the KE distribution, suggesting that the electron temporarily trapped in the shape

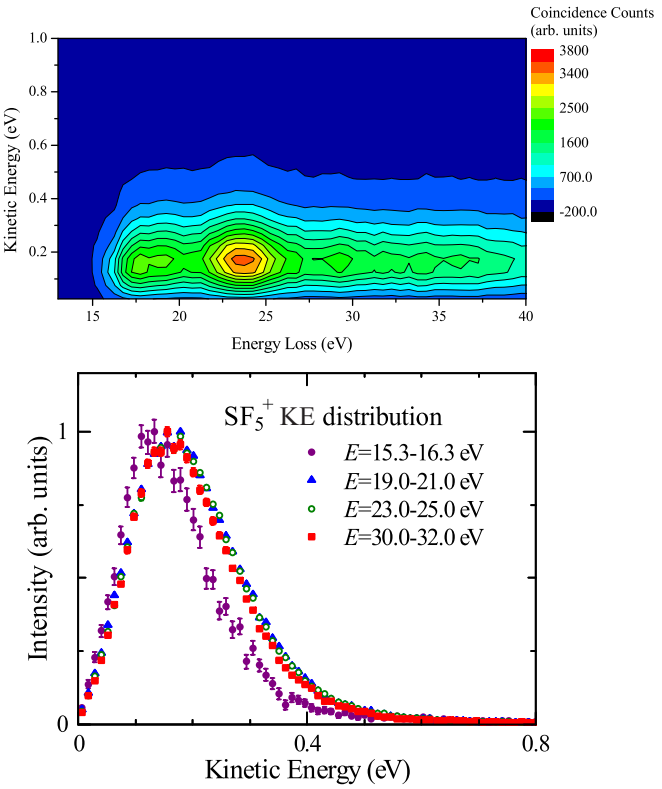

FIG. 4. The upper panel is the E-KE correlation map of SF_5^+ and the lower panel compares the KE distributions for different electron energy loss regions.

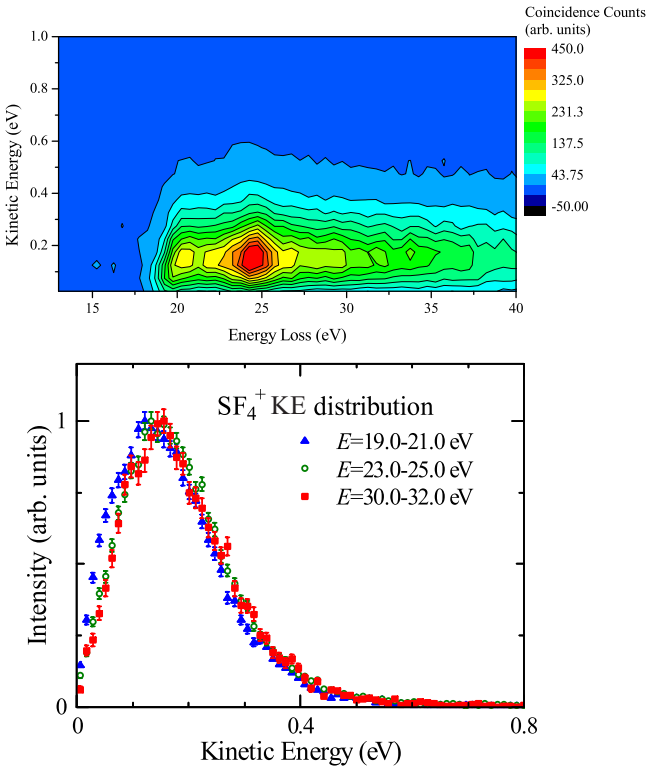

FIG. 5. The upper panel is the E-KE correlation map of SF_4^+ and the lower panel compares the KE distributions for different electron energy loss regions.

resonance is rapidly released before the dissociation. The low intensity in the small-KE region is due to the fact that the SF_5^+ ions are generated by the direct dissociation of SF_6^+ and thus receive a large recoil momentum. The results are in good agreement with the KE distribution of SF_5^+ produced by 100 eV electron impact [25], while scattered electrons were not measured in that study. The agreement is consistent with the observation that the KE distribution is insensitive to E and K^2.

A closer look at Fig. 4 shows that the KE distribution at $E = 15.3 - 16.3$ eV, where only the $X\ ^2T_{1g}$ state is accessible, has a maximum at lower energy, 0.13 eV. This indicates that SF_5^+ ions originating from the $X\ ^2T_{1g}$ state have a slightly lower average KE than those from the higher SF_6^+ states. In the direct dissociation of $SF_6^+ \rightarrow SF_5^+ + F$, the recoil energy gained by F should be 0.87 eV when the KE of SF_5^+ is 0.13 eV due to the conservation law of $\boldsymbol{p}_1 = -\boldsymbol{p}_2$, where $\boldsymbol{p}_1$ and $\boldsymbol{p}_2$ are the momenta of SF_5^+ and F, respectively. The obtained kinetic energy release (KER), 1.0 eV, is in excellent agreement with the mean KER, 0.99 ± 0.01 eV, reported in the TPEPICO study by Creasey *et al.* [16]. However, the mean KE calculated using the experimental KE distribution, 0.17 eV, is slightly higher than the energy of the maximum due to the asymmetry of the distribution; accordingly, the mean KER derived from this value, 1.3 eV, is higher than the result of the TPEPICO study. In the following discussion, the position of the maximum of each KE distribution is mainly used because it can be considered as the most probable KE value and also because the average KE of a given ionization channel cannot be obtained when two or more channels contribute to an experimental KE distribution. The energy of $SF_5^+ + F$ has been thermodynamically determined to be 14.0 eV with respect to the ground-state energy of SF_6 [15,16]. The available energy of the $X\ ^2T_{1g}$ state is thus deduced to be ~ 1.7 eV from the ionization energy of 15.7 eV, and our result shows that 59% of it is partitioned into the relative translational energy of the fragments. This is much higher than the 22% found in *ab initio* dynamical calculations [33], but is in fair agreement with the value of 72% obtained using an impulsive dissociation model [34], in which the ratio of the mean KER to the available energy is given by $\mu_{S\text{-}F}/\mu_{SF_5\text{-}F}$, where $\mu_{X\text{-}Y}$ indicates the reduced mass of X-Y.

From the TPEPICO results, the mean KEs of SF_5^+ ions for the $\{A, B, {}^2T_{1u}, {}^2T_{2u}\}$ and $C\ ^2E_g$ channels are obtained to be 0.16 ± 0.01 and 0.17 ± 0.01 eV, respectively [16]. The values are in good accordance with the maximum position of the KE distributions at $E >\sim 18$ eV, but smaller than the mean KE derived from the distributions, 0.20 eV. It is worth noting that although the mean KER of the dissociation from the $\{A, B, {}^2T_{1u}, {}^2T_{2u}\}$ and $C\ ^2E_g$ states, 1.2–1.3 eV [16], is slightly higher than that from the $X\ ^2T_{1g}$ state, $\sim$1.0 eV, its increase is much smaller than the increase in ionization energy. This indicates that the excess energies of the higher SF_6^+ states are partially released before the dissociation. Since SF_6^+ states with a hole in an outer-valence level do not decay radiatively [35], the energy release should be due to internal conversion to a lower electronic state in SF_6^+, as pointed out by Creasey *et al.* [16] and Peterka *et al.* [18].

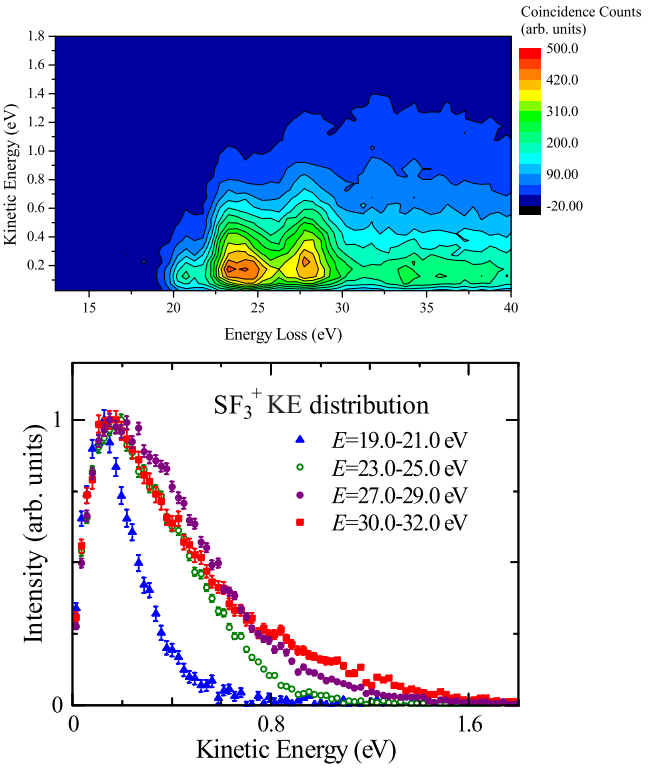

FIG. 6. The upper panel is the E-KE correlation map of SF_3^+ and the lower panel compares the KE distributions for different electron energy loss regions.

The KE distribution of SF_4^+ is then considered in Fig. 5. As in the case of SF_5^+, it shows little E dependence and resembles the result of the electron-impact study by Bull *et al.* [25]. A comparison with the results for SF_5^+ reveals that SF_4^+ ions, which are predominantly produced by the $D\ ^2T_{2g}$ ionization, have a KE distribution similar to that of SF_5^+ ions, suggesting some similarity between the dissociation mechanisms of the $D\ ^2T_{2g}$ state and higher SF_6^+ states. The decay mechanism of the $D\ ^2T_{2g}$ state will be discussed later.

In contrast to the cases of SF_5^+ and SF_4^+, a significant E dependence of the KE distribution has been observed for SF_3^+, as can be seen in Fig. 6. Among the SF_6^+ states that can yield SF_3^+, only $D\ ^2T_{2g}$ is accessible at $E = 19 - 21$ eV, and the KE distribution in this E region has a maximum at ~ 0.13 eV and extends to ~ 0.7 eV. Figure 6 shows that the KE distribution changes significantly around $E = 22$ eV, at which SF_3^+ arises also from the $E\ ^2T_{1u}$ state, reflecting the difference between the dissociation mechanisms of the $D\ ^2T_{2g}\ (1t_{2g})^{-1}$ and $E\ ^2T_{1u}\ (4t_{1u})^{-1}$ states; it has a shoulder at $\sim$0.33 eV and extends to above 1.0 eV. The shoulder is more pronounced in the KE distribution for $E = 27 - 29$ eV due to the enhancement of the $E\ ^2T_{1u}$ ionization caused by the $4t_{1u} \rightarrow \varepsilon t_{2g}$ shape resonance. The associated $1t_{2g}$ and $4t_{1u}$ orbitals have F $2p$ nonbonding and S-F bonding characters, respectively, and it is likely that the difference in orbital character significantly affects the fragmentation mechanism. According to the PEPICO study by Stankiewicz *et al.* [17], SF_3^+ is also generated from the $F\ ^2A_{1g}$ state. Indeed, the high-energy component of the KE distribution increases above approximately the corresponding ionization energy of 26.8 eV, and this would be due to the contribution of the $F\ ^2A_{1g}$ ionization. It has been shown by TPEPICO experiments that the $D\ ^2T_{2g}$ and $E\ ^2T_{1u}$ states yield SF_5^+ with mean KEs of 0.16 ± 0.02 and 0.39 ± 0.02 eV, respectively [16], which are in reasonable accordance with the positions of the peak and shoulder observed in the KE distributions. The 100 eV electron-impact experiments by Bull *et al.* [25] have shown that two shoulders appear at 0.16 and 0.35 eV in the KE distribution of SF_3^+ due to the $D\ ^2T_{2g}$ and $E\ ^2T_{1u}$ ionization, respectively. In addition to these features, a dominant maximum was observed at 0.03 eV and attributed to statistical dissociation with a longer timescale. In contrast, no significant contribution of SF_3^+ ions with such low KE was found in the present measurements. Although our KE distributions are slightly broadened due to the thermal energy of the target molecules, a considerable intensity should be observed at ~ 0.03 eV if there is a strong peak as reported in the literature. While it has been argued that the shape resonance observed in the SF_3^+ yield spectrum is a possible origin of the statistical-like signal [25], no enhancement of the low-KE component was observed at $E \sim 28$ eV, where the $4t_{1u} \rightarrow \varepsilon t_{2g}$ transition occurs.

It is noteworthy that the KE distribution of SF_3^+ at $E = 19-21$ eV, where only the $D\ ^2T_{2g}$ state is accessible, is similar to that of SF_5^+. This tendency was observed also for SF_4^+. The results strongly suggest that there is some similarity between the decay mechanisms of the $D\ ^2T_{2g}$ state and lower SF_6^+ states. The observations can be explained by a mechanism in which the $D\ ^2T_{2g}$ state internally converts to a lower electronic state and impulsive dissociation occurs to form SF_5^+, as in the case of the $\{A, B, {}^2T_{1u}, {}^2T_{2u}\}$ and $C\ ^2E_g$ states; then F or F_2 is statistically emitted from SF_5^+. For the SF_4^+ formation, this mechanism has also been proposed in other studies [16,18,25], but Stankiewicz *et al.* [17] suggested that the favorable channel is the $SF_4^+ + F_2$ single-step decomposition. If the above argument is correct, the velocities of the SF_4^+ and SF_3^+ ions should be close to the velocity of SF_5^+ before the dissociation, since the statistical loss of F or F_2 would have only a small effect on the motion of the product. Figure 7 compares the velocity distributions of the fragment ions. First, the SF_4^+ yield is discussed. It is clear from the figure that the velocity distribution of SF_4^+ is in good agreement with that of SF_5^+ at $E = 23-25$ and 30–32 eV, as expected. The same is true for higher-E regions (data are not shown), strongly supporting the above argument. The only exception is the result at $E = 19-21$ eV, where some difference between the KE distributions of SF_4^+ and SF_5^+ is observed on the low-KE side [see Fig. 7(a)]. This may be due to the fact that ionization in the low-E region has a high probability of leading to the formation of the $D\ ^2T_{2g}$ state on the low-energy part of the potential energy surface, where only a smaller energy can be partitioned into the relative translational energy of SF_5^+ and F.

For further discussion, a schematic energy diagram is shown in Fig. 8. As mentioned above, the KER distribution of the dissociation to $SF_5^+ + F$ is insensitive to the parent ion state, and its maximum appears at about 1.0–1.3 eV. Thus it can be deduced that when the $D\ ^2T_{2g}$ state with the energy of 19.8 eV decays to $SF_5^+ + F$, the total internal energy of the fragments is $19.8\ \text{eV} - (1.0 \sim 1.3\ \text{eV}) = 18.8 \sim 18.5$ eV,

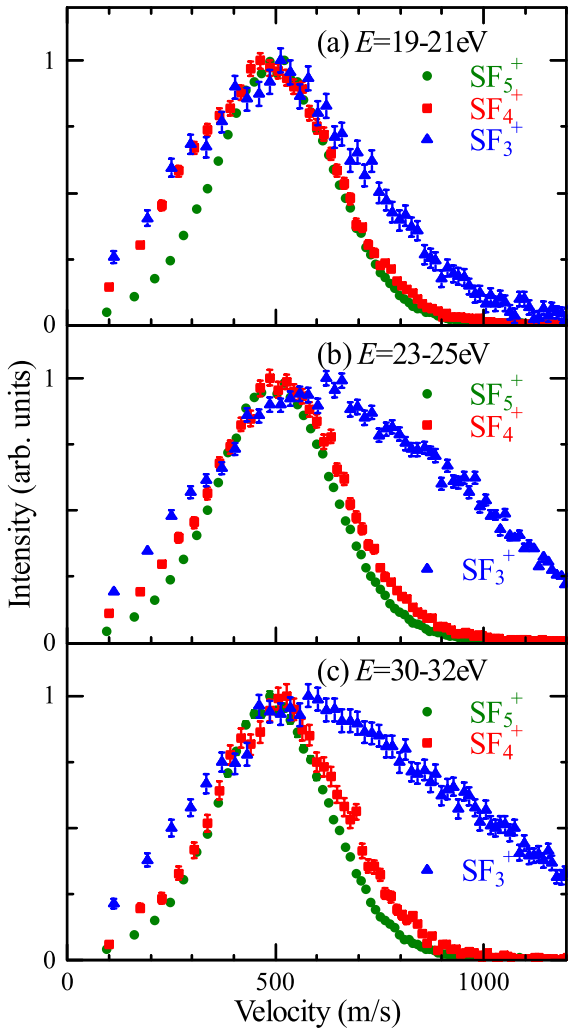

FIG. 7. Velocity distributions of SF_5^+, SF_4^+, and SF_3^+ for $E =$ (a) $19-21$, (b) $23-25$, and (c) $30-32$ eV.

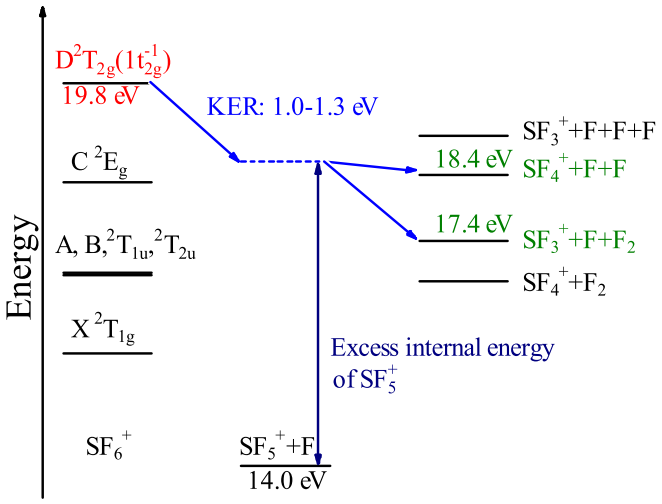

FIG. 8. Schematic energy level diagram. The energies in the figure are with respect to the ground-state energy of SF_6. The values for the dissociation limits are taken from Refs. [15,16]. The energy of $SF_5^+ + F$ formed from the $D\ ^2T_{2g}$ state, which includes the high internal energy of SF_5^+ (see text for details), is depicted as a dashed line.

which is slightly higher than the energy of $SF_4^+ + F + F$, 18.4 eV [15,16]. The decomposition of SF_5^+ may therefore occur to release its excess internal energy. Because of the small energy difference between $SF_5^+ + F$ and $SF_4^+ + F + F$, SF_4^+ receives only a small amount of recoil kinetic energy, and its velocity should be close to that of SF_5^+, which is indeed observed in Fig. 7. It should be noted that although the single-step dissociation to $SF_4^+ + F_2$ (16.8 eV) is also energetically accessible from the $D\ ^2T_{2g}$ state, it is unlikely that the velocity distribution of SF_4^+ produced by this mechanism shows the remarkable similarity to that of SF_5^+.

The energy diagram also shows that there is a dissociation limit of $SF_3^+ + F_2 + F$ at 17.4 eV, and thus SF_5^+ produced in the first-step dissociation can decay not only to $SF_4^+ + F$ but also to $SF_3^+ + F_2$. Since the latter is ~ 1.0 eV lower in energy than the former, SF_3^+ can receive a higher recoil kinetic energy than SF_4^+. Depending on the recoil direction, the gained kinetic energy causes the velocity of SF_3^+ in the laboratory frame to increase or decrease compared to the velocity of SF_5^+ before the dissociation. Thus, if this decay mechanism is dominant, SF_3^+ should have a wider velocity distribution than SF_5^+, while their mean KEs would be almost identical. The result of SF_3^+ in Fig. 7(a) is in good accordance with this expectation and strongly supports the above decay mechanism. On the other hand, the KE distributions of SF_3^+ in Figs. 7(b) and 7(c) are significantly different from those of SF_5^+ and SF_4^+ in the high-velocity region due to the contribution of the $E\ ^2T_{1u}$ and $F\ ^2A_{1g}$ channels.

C. Angular distribution of SF_5^+

Since SF_5^+ is produced by the direct decomposition of SF_6^+ on a shorter timescale compared to the molecular rotation period [33], its recoil direction closely coincides with the S-F bond direction at the moment of electron collision. Thus the angular dependence of the SF_5^+ emission carries information on the stereodynamics of the electron-impact ionization. Figure 9 shows the SF_5^+ angular distributions for $E = 22-24$ eV at $K^2 = 0.16$ and 0.66 a.u., which are obtained by plotting the number of electron-SF_5^+ coincidence signals as a function of the angle between the ion recoil momentum and the momentum transfer vector, ϕ_K. For higher K^2, large statistical errors prevent a meaningful investigation of the angular anisotropy and the data are therefore not shown. The experimental results are fitted to an analytical expression of $c[1 + \beta_2 P_2(\cos\phi_K) + \beta_4 P_4(\cos\phi_K)]$ [27,28], where $P_2(\cos\phi_K)$ and $P_4(\cos\phi_K)$ are the second- and fourth-order Legendre polynomials. The values of c, β_2, and β_4 were optimized by least-squares fitting. The data in the figure have been scaled to make c equal to 1 for ease of comparison. Angular distributions were also constructed for other ions and found to be isotropic within the experimental uncertainty.

It can be seen from Fig. 9(a) that the SF_5^+ angular distribution at $K^2 = 0.16$ a.u. shows a shallow minimum at $\phi_K = 90^\circ$ and has maxima at 0° and 180°. A similar tendency is observed in other E regions. While the angular anisotropy is observed in electron-impact ionization, it is much smaller than that for SF_5^+ produced by photoionization [18,36]. For

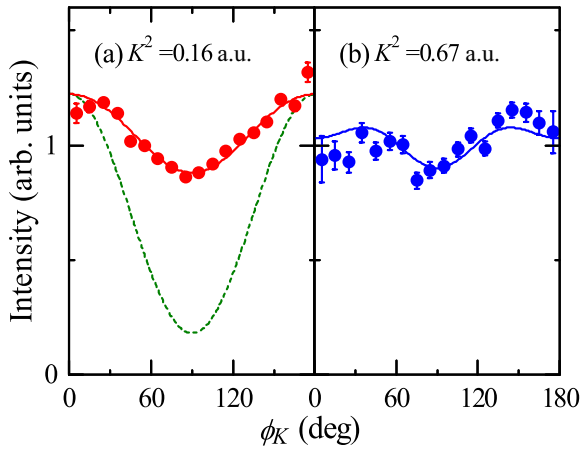

FIG. 9. Angular distribution of SF_5^+ for $E = 22 - 24$ eV at $K^2 =$ (a) 0.16 and (b) 0.67 a.u. Solid lines are an analytical function fitted to the experimental data, $c[1 + \beta_2 P_2(\cos\phi_{\boldsymbol{K}}) + \beta_4 P_4(\cos\phi_{\boldsymbol{K}})]$, and the dashed line is the associated photoion angular distribution at a photon energy of 23.2 eV, $c'[1 + \beta P_2(\cos\phi)]$ with $\beta = 1.31$ [18]. For ease of comparison, the photoion angular distribution is scaled to make the intensity at 0° equal to that of the fitted function.

comparison, the photoion angular distribution at a photon energy of 23.2 eV [18] is depicted as a dashed line. It is expressed as $c'[1 + \beta P_2(\cos\phi)]$, where β is the so-called anisotropy parameter and ϕ is the angle made between the light polarization vector and ion recoil momentum. At $K \sim 0$, the GOS coincides with OOS and $\boldsymbol{K}$ plays a role equivalent to the light polarization vector in photoionization as mentioned in Sec. II. Thus the dashed line corresponds to the SF_5^+ angular distribution at zero momentum transfer. It is clear from the figure that the angular anisotropy is significantly reduced by increasing K^2 from 0 to 0.16 a.u., indicating that quadrupole and higher-order multipole interactions make the ionization cross section less sensitive to the orientation of SF_6. Figure 9(b) shows that a further increase of K^2 to 0.67 a.u. causes the decrease of the relative intensities at $\phi_{\boldsymbol{K}} = 0°$ and 180°. The experiments reveal that the stereodynamics of the electron-impact ionization of SF_6 quickly changes from the dipole regime with the increase of momentum transfer.

IV. SUMMARY

In this work, the electron-impact dissociative ionization of SF_6 has been studied in detail using $(e, e + \text{ion})$ spectroscopy. The total and partial ion-yield spectra have been obtained on the absolute scale at four different scattering angles to investigate the change of ion production with momentum transfer. Shape resonance features have been observed in the spectra and their assignments and momentum transfer dependence have been discussed. The results reveal that the $4t_{1u} \rightarrow \varepsilon t_{2g}$ shape resonance band is quite distinct over a wide momentum transfer range and has a significant influence on the SF_3^+ formation by electron impact, while the other shape resonance bands show a typical behavior of dipole-allowed transitions in which the intensity decreases rapidly with K^2.

The E-KE correlation maps of the fragment ions have been constructed to discuss the molecular fragmentation mechanisms of SF_6^+. The peak and shoulder positions of the ion KE distributions are in general agreement with the mean KE values reported in photodissociative ionization studies. No influence of shape resonance has been observed in the analysis, suggesting that the electron temporarily trapped by a barrier in the effective molecular potential is rapidly released prior to the bond dissociation. The KE distributions of SF_5^+ and SF_4^+ show little E dependence and resemble each other. In addition, the KE distribution of SF_3^+ produced by the $D\ ^2T_{2g}$ ionization is found to be similar to that of SF_5^+. The results strongly suggest that many of the parent ions in the $D\ ^2T_{2g}$ state internally convert to a lower electronic state, followed by impulsive dissociation to form SF_5^+; then the high internal energy of SF_5^+ is liberated by statistical emission of F or F_2. This mechanism is supported by the remarkable similarity between the velocity distributions of the SF_5^+, SF_4^+, and SF_3^+ ions.

It is also found that there is a significant difference between the angular distributions of SF_5^+ ions produced by photoionization and electron-impact ionization, in contrast to the consistency of the KE distributions. The strong angular anisotropy observed in photodissociative ionization is significantly reduced even at small momentum transfer, indicating that the stereodynamics of the electron-impact ionization of SF_6 changes rapidly from that in the dipole regime due to the influence of electric quadrupole and higher-order multipole interactions.

The present study has demonstrated that the $(e, e + \text{ion})$ technique is a powerful tool to investigate the dynamics of electron-impact dissociative ionization of molecules and also to elucidate the influence of nondipole interactions. Furthermore, the results provide fundamental knowledge for understanding the behavior of SF_6 in industrial applications such as plasma etching.

ACKNOWLEDGMENTS

This research was supported by Grants-in-Aid for Scientific Research (KAKENHI, Grants No. 19K21862, No. 21H01874, No. 21H04672, and No. 21K18926) from the Japanese Ministry of Education, Culture, Sports, Science, and Technology, Japan. It was also supported in part by the "Five-Star Alliance."

[1] B. Wu, A. Kumar, and S. Pamarthy, High aspect ratio silicon etch: A review, J. Appl. Phys. **108**, 051101 (2010).

[2] V. M. Donnelly and A. Kornblit, Plasma etching: Yesterday, today, and tomorrow, J. Vac. Sci. Technol. A **31**, 050825 (2013).

[3] G. Kokkoris, A. Panagiotopoulos, A. Goodyear, M. Cooke, and E. Gogolides, A global model for SF_6 plasmas coupling reaction kinetics in the gas phase and on the surface of the reactor walls, J. Phys. D: Appl. Phys. **42**, 055209 (2009).

[4] L. G. Christophorou and J. K. Olthoff, Electron interactions with SF_6, J. Phys. Chem. Ref. Data **29**, 267 (2000), and references therein.

[5] B. Goswami and B. Antony, Electron impact scattering by SF_6 molecule over an extensive energy range, RSC Adv. **4**, 30953 (2014), and references therein.

[6] D. M. P. Holland, M. A. MacDonald, P. Baltzer, L. Karlsson, M. Lundqvist, B. Wannberg, and W. von Niessen, An experimental and theoretical study of the valence shell photoelectron spectrum of sulphur hexafluoride, Chem. Phys. **192**, 333 (1995).

[7] J. T. Francis, C. C. Turci, T. Tyliszczak, G. G. B. de Souza, N. Kosugi, and A. P. Hitchcock, Electron-impact core excitation of SF_6. I. S $2p$, S $2s$, and F $1s$ spectroscopy, Phys. Rev. A **52**, 4665 (1995).

[8] M. Stener, D. Toffoli, G. Fronzoni, and P. Decleva, Time dependent density functional study of the photoionization dynamics of SF_6, J. Chem. Phys. **124**, 114306 (2006).

[9] J. Jose, R. R. Lucchese, and T. N. Rescigno, Interchannel coupling effects in the valence photoionization of SF_6, J. Chem. Phys. **140**, 204305 (2014).

[10] J. Jose and R. R. Lucchese, Vibrational effects in the shape resonant photoionization leading to the $A\ ^2T_{1u}$ state of SF_6, Chem. Phys. **447**, 64 (2015).

[11] E. Plésiat, S. E. Canton, J. D. Bozek, P. Decleva, and F. Martín, Resonant photoelectron confinement in the SF_6 molecule, J. Phys. Chem. A **123**, 1062 (2019).

[12] A. P. Hitchcock and M. J. van der Wiel, Absolute oscillator strengths (5–63 eV) for photoabsorption and ionic fragmentation of SF_6, J. Phys. B: At., Mol. Phys. **12**, 2153 (1979).

[13] T. Masuoka and J. A. R. Samson, Dissociative and double photoionization of SF_6 in the 75–125 eV region, J. Chem. Phys. **75**, 4946 (1981).

[14] I. G. Simm, C. J. Danby, J. H. D. Eland, and P. I. Mansell, Translational energy release in the loss of fluorine atoms from the ions SF_6^+, CF_4^+ and $C_2F_6^+$, J. Chem. Soc. Faraday Trans. II **72**, 426 (1976).

[15] J. C. Creasey, I. R. Lambed, R. P. Tuckett, K. Codling, L. J. Frasinski, P. A. Hatherly, and M. Stankiewicz, Fragmentation of valence electronic states of SF_6 studied with synchrotron radiation, J. Chem. Soc. Faraday Trans. **87**, 1287 (1991).

[16] J. C. Creasey, H. M. Jones, D. M. Smith, R. P. Tuckett, P. A. Hatherly, K. Codling, and I. Powis, Fragmentation of valence electronic states of CF_4^+ and SF_6^+ studied by threshold photoelectron-photoion coincidence spectroscopy, Chem. Phys. **174**, 441 (1993).

[17] M. Stankiewicz, J. Rius i Riu, J. Álvarez Ruiz, P. Erman, P. Hatherly, A. Kivimäki, E. Melero García, and E. Rachlew, Relaxation dynamics of SF_6 studied by energy-resolved electron ion coincidence technique, J. Electron Spectrosc. Relat. Phenom. **137-140**, 369 (2004).

[18] D. S. Peterka, M. Ahmed, C.-Y. Ng, and A. G. Suits, Dissociative photoionization dynamics of SF_6 by ion imaging with synchrotron undulator radiation, Chem. Phys. Lett. **312**, 108 (1999).

[19] M. Inokuti, Inelastic collisions of fast charged particles with atoms and molecules—the Bethe theory revisited, Rev. Mod. Phys. **43**, 297 (1971).

[20] K. T. Leung, Valence and inner shell non-dipole excitation spectroscopy of polyatomic molecules by angle-resolved inelastic electron scattering at high energy, J. Electron Spectrosc. Relat. Phenom. **100**, 237 (1999).

[21] N. Watanabe, T. Hirayama, D. Suzuki, and M. Takahashi, Vibronic effects on the low-lying electronic excitations in CO_2 induced by electron impact, J. Chem. Phys. **138**, 184311 (2013).

[22] J. F. Ying, T. A. Daniels, C. P. Mathers, H. Zhu, and K. T. Leung, Absolute transition probability measurement of nondipole valence-shell (7–70 eV) electronic transitions of SF_6 by angle-resolved electron energy loss spectroscopy, J. Chem. Phys. **99**, 3390 (1993).

[23] N. Watanabe, T. Hirayama, and M. Takahashi, Vibrational effects on electron-impact valence excitations of SF_6, Phys. Rev. A **99**, 062708 (2019).

[24] I. G. Eustatiu, J. T. Francis, T. Tyliszczak, C. C. Turci, A. L. D. Kilcoyne, and A. P. Hitchcock, Generalized oscillator strengths for inner-shell excitation of SF_6 recorded with a high-performance electron energy loss spectrometer, Chem. Phys. **257**, 235 (2000).

[25] J. N. Bull, J. W. L. Lee, and C. Vallance, Electron-impact-ionization dynamics of SF_6, Phys. Rev. A **96**, 042704 (2017).

[26] N. Watanabe, S. Yamada, and M. Takahashi, Molecular-frame electron-scattering experiment on the dipole-forbidden $2\sigma_g \rightarrow 1\pi_g$ transition of N_2, Phys. Rev. A **95**, 060702(R) (2017).

[27] N. Watanabe, S. Yamada, and M. Takahashi, Stereodynamics of electron-induced dissociative ionization of N_2 studied by $(e, e +$ ion) spectroscopy, Phys. Chem. Chem. Phys. **20**, 1063 (2018).

[28] N. Watanabe, S. Yamada, and M. Takahashi, $(e, e +$ ion) study on electron-induced dissociative ionization of O_2, Phys. Rev. A **99**, 022704 (2019).

[29] N. Watanabe and M. Takahashi, Forward–backward asymmetry in electron impact ionization of CO, J. Chem. Phys. **152**, 164301 (2020).

[30] N. Watanabe and M. Takahashi, Symmetry breaking in electron-impact dissociative ionization of linear symmetric molecules, Phys. Rev. A **104**, 032812 (2021).

[31] N. Watanabe, T. Hirayama, S. Yamada, and M. Takahashi, Development of an electron-ion coincidence apparatus for molecular-frame electron energy loss spectroscopy studies, Rev. Sci. Instrum. **89**, 043105 (2018).

[32] G. Bieri, L. Åsbrink, and W. von Niessen, 30.4-nm He(II) photoelectron spectra of organic molecules: Part VII. Miscellaneous compounds, J. Electron Spectrosc. Relat. Phenom. **27**, 129 (1982).

[33] H. Tachikawa, The ionization dynamics of SF_6: A full dimensional direct *ab initio* dynamics study, J. Phys. B: At., Mol. Opt. Phys. **33**, 1725 (2000).

[34] I. Powis, The dissociation of state-selected $CF_3\,X^+$ molecular ions, Mol. Phys. **39**, 311 (1980).

[35] T. Field and J. H. D. Eland, Light emissions accompanying molecular ionization, Chem. Phys. Lett. **197**, 542 (1992).

[36] M. Ono and K. Mitsuke, Anisotropy of fragment ions from SF_6 by photoexcitation between 23 and 210 eV, Chem. Phys. Lett. **366**, 595 (2002).